Electrode Engineering in Memristors Development for Non-/Erasable Storage, Random Number Generator, and Synaptic Applications

Firman Mangasa Simanjuntak
School of Electronics & Computer Science
University of Southampton
Southampton, SO17 1BJ, U.K.
f.m.simanjuntak@soton.ac.uk

Fayzah Talbi
Department of Physics
University of York
York, YO10 5DD, U.K.

Adam Kerrigan
Department of Physics
University of York
York, YO10 5DD, U.K.

Vlado K. Lazarov
Department of Physics
University of York
York, YO10 5DD, U.K.

Themistoklis Prodromakis
School of Engineering
University of Edinburgh
Edinburgh, EH9 3FB, U.K.

***Abstract*—We report the process development of ZnO-based memristors and observe various switching phenomena by means of electrode engineering, such as digital-to-analogue transformation, irregular and uniform endurance, and non-erasable switching; we also discuss the potential applications for each of these switching phenomena. The use of inert electrodes induces a high injection of electrons into the switching layer triggering abrupt current changes and, in some cases, resulting in a device breakdown. Meanwhile, a low work function and oxidizable electrode encourage Ohmic contact at the oxide/electrode junction and exhibit gradual switching characteristics. This work addresses the importance of electrode configuration to achieve the desired switching behaviour for specific low-powered electronic applications.**

Keywords—memristor, WORM, data storage, random number generator, synaptic, resistive memory, semiconductor fabrication.

I. Introduction

Memristor technology is a promising candidate for future memory applications [1]. A memristor cell consists of a metal/insulator/metal sandwich configuration, and this simple device structure is beneficial for making ultra-high-density storage [2]. The working mechanism of a memristor is based on an electric field-induced electrochemical reaction [3]. The formation/rejuvenation and rupture of a conductive channel that connects the cathode and anode lead to the occurrence of low (LRS, On) and high resistance states (HRS, Off), respectively [4]. The process where the device switches from HRS to LRS is called Set; conversely, LRS to HRS is called Reset [5]. This conduction channel can be an arrangement of metal cations, oxygen vacancies (Vo) or a mixture of these defects [6]. An active metal electrode, such as Ag, can act as a metal cation supplier for the formation of a metallic-based channel called a conducting bridge (AgCB) [7]. However, the device made with inert (or inactive) electrodes is controlled by a channel that is called oxygen vacancy conducting filament (VoCF) [8].

Ideally, the memristor device should be able to perform repeated set-reset processes to ensure the device is suitable for a memory component [9]. Nevertheless, the device that can only be switched once (unable to reset or cannot be switched off) is also useful for non-erasable data storage [10]. Nowadays, a memristor can be used for applications beyond data storage [11]. For example, a memristor showing analogue switching is able to mimic the synaptic response of mammalian neuronal systems and could be used for neuromorphic computing elements [12]; neuromorphic computing is a new paradigm that could revolutionize the traditional Von Neumann computer architecture [13]. Another interesting application is for data security; in principle, the ionic movement and redox reaction in the memristor cell is unpredictable, which may result in random states (data) [14]. Henceforth, unstable devices could still be useful for generating random data [15].

II. Methods

A. Device Fabrication

Wafer-scale device fabrication was conducted employing the photolithography technique to fabricate a cross-point array device structure, and the process flow is depicted in Fig. 1(a). A negative photoresist (PR) was spin-coated onto SiO_2-coated Si wafers, then exposed to ultraviolet light, and developed to pattern bottom electrodes (Fig. 1(a)(i)); then, Pt and TiN bottom electrodes (BE) were deposited (Fig. 1(a)(ii)) and followed by a lift-off process (Fig. 1(a)(iiii)), note that a thin layer of Ti was deposited prior the BE deposition as an adhesion layer. Before switching layer (SL) deposition, the PR was coated the BE pads to ensure no switching layer was deposited on the pads area (Fig. 1(a)(iv)); hereafter, the rest of the region was covered with the ZnO SL and followed by a lift-off process to remove the PR and ZnO film on the BE pads (Figs. 1(a)(v) and (vi)). Following the same procedure described in Figs. 1(a)(i-iii), the Pt/Ag, Au/Ag or Au top electrodes (TE) were patterned onto the oxide to fabricate metal/insulator/metal (MIM) structure (Figs. 1(a)(vii-ix)). Note that a thin Pt or Au metal were deposited onto the Ag TE as a capping layer to enhance the conductivity of the top electrode and to avoid surface oxidation (AgOx). The metal deposition (Pt, Ag, and Au) was conducted using an evaporation technique (Lab 700, Leybold Optics GmbH); meanwhile, ZnO and TiN were deposited using a sputtering technique from ZnO and Ti targets, respectively (Angstrom Engineering Inc.).

B. Structural Observation and Electrical Analysis

Fig. 1(b) shows the optical micrograph of the fabricated 5 x 5 μm memristor cross-point array (YR Nikon microscope), and the photograph of the arrays on a 6-inch wafer is shown

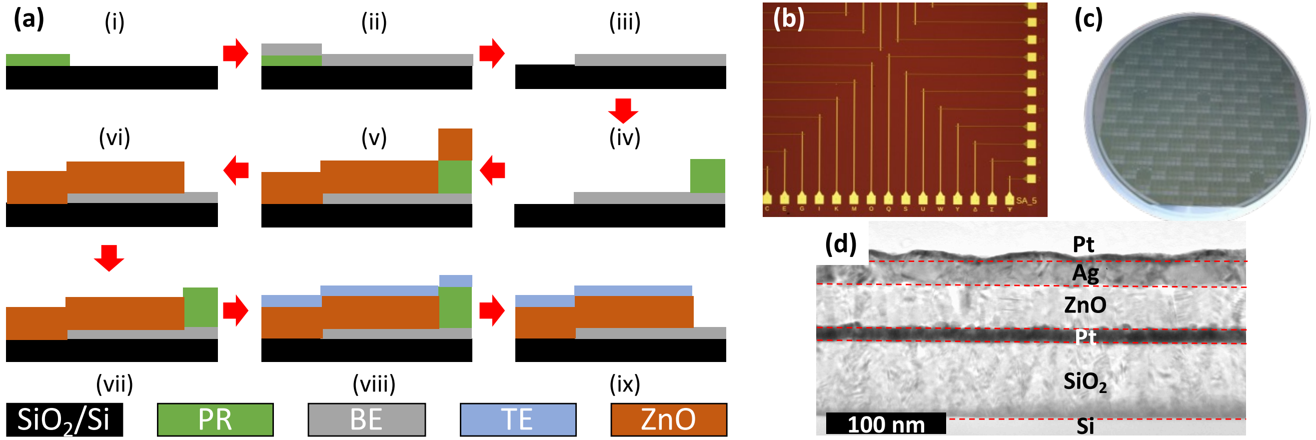

Fig. 1. Device fabrication and structural observation of the memristor devices. (a) Lithography and film depositions process flow, (b) Optical micrograph of the cross-point array, (c) Photograph of the memristor arrays fabricated on 6-inch wafer, and (d) A representative TEM image of the fabricated devices (Ag/ZnO/Pt).

in Fig. 1(c). A transmission electron microscope (TEM, JEOL JEM-2100Plus) was used to observe the structure of the device, Fig. 1(d) depicts a cross-sectional TEM image of the Ag (30 nm)/ZnO (60 nm)/Pt (25 nm) MIM device structure. The electrical characteristics of the devices were measured by applying negative or positive voltage pulses on the top electrode while the bottom electrode was grounded (ArCOne, ArC Instruments, Ltd.)

III. Results and Discussions

Fig. 2 shows the typical I-V curves of Ag (30nm) /ZnO (60 nm)/Pt (25 nm) and Ag (30 nm)/ZnO (60 nm)/TiN (60 nm) devices. The devices exhibit a counter-clockwise switching behaviour where the set and reset processes require positive and negative voltage biases, respectively. The devices made with Pt bottom electrodes have an On/Off ratio of more than two orders of magnitude and abrupt current rise and fall during the set and reset, respectively (Fig. 2(a)). Meanwhile, the ones with TiN electrodes have approximately one order of magnitude and gradual current change during the set and reset processes (Fig. 2(b)). The abrupt current changes in Ag/ZnO/Pt device indicate a digital switching characteristic. Digital switching is suitable for data storage applications since it tends to perform a high On/Off ratio [16], allowing a small and efficient sense amplifier for making cost-efficient circuits [17]; however, it is less favourable for making synaptic devices due to the difficulty to control the resistance states employing various voltages or number of pulses [18]. On the other hand, the gradual switching observed in the Ag/ZnO/TiN indicates analogue behaviour that has the potential for making synaptic devices [19].

We suggest that the formation of the TiON interfacial layer between the SL and BE films are responsible for the analogue behaviour in Ag/ZnO/TiN device. The Gibbs free energy of oxide formation (ΔG^0) of TiON (-580.3 kJ/mol) [20] is lower than that of ZnO (-350 kJ/mol) [21]; hence, the formation of TiON interfacial layer can be easily formed during the ZnO deposition where the TiN absorbs oxygen from ZnO. The TiON could enhance the ohmic contact at ZnO/TiN interface; moreover, ZnO/TiN junction has a low barrier height considering the work function of TiN is 4.4 eV

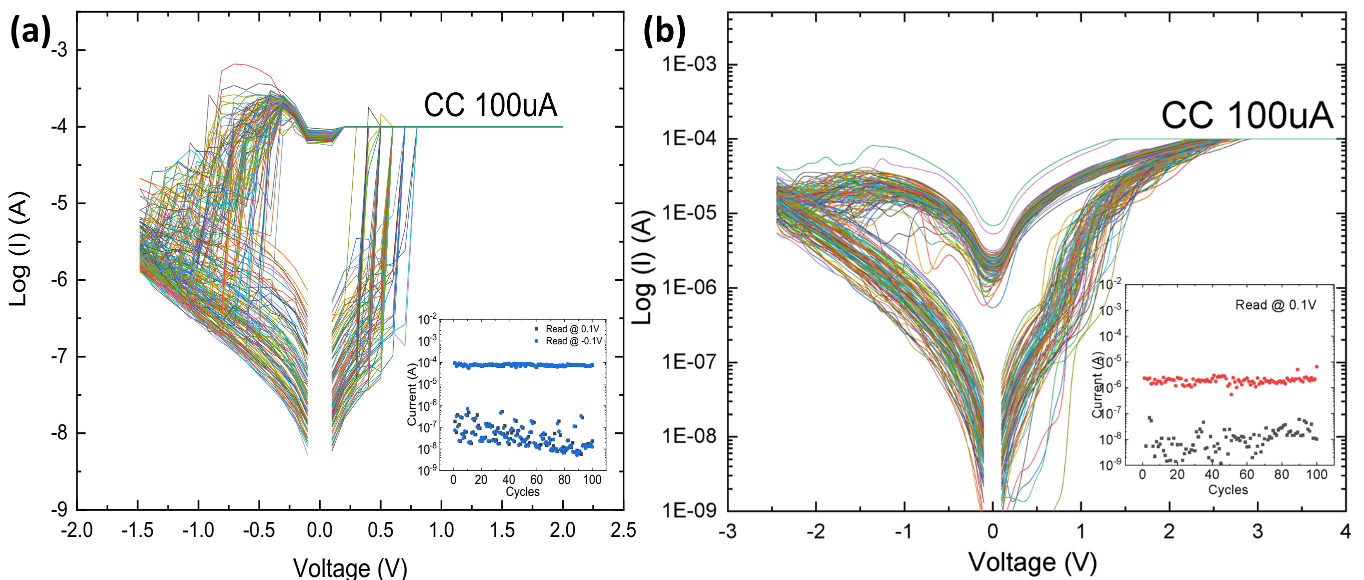

Fig. 2. Typical I-V curves of (a) Ag/ZnO/Pt and (b) Ag/ZnO/TiN devices.

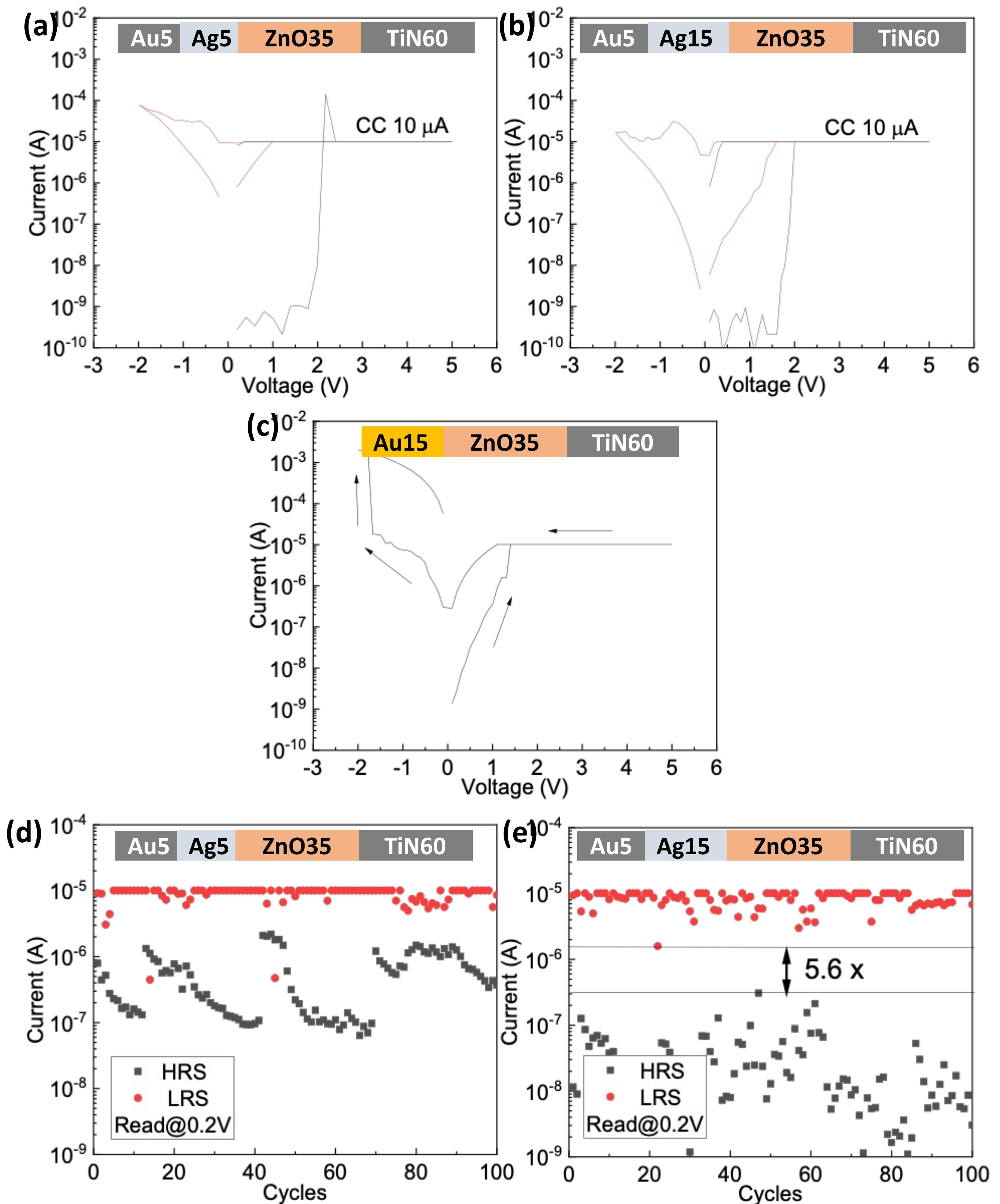

Fig. 3. Typical I-V curves of (a) Au (5 nm)/Ag (5 nm)/ZnO (35 nm)/TiN (60 nm), (b) Au (5 nm)/Ag (15 nm)/ZnO (35nm)/TiN (60 nm) and (c) Au (15 nm)/ZnO (35 nm)/TiN (60 nm). (d) and (e) Endurance performance of (a) and (b), respectively.

[22] and the electron affinity of ZnO is 4.35 eV [23]. This configuration could induce a gradual electron injection from the electrode to the switching layer. Meanwhile, the Pt has a work function of 5.65 eV [24], which could result in a Schottky contact due to the large barrier height at the ZnO/Pt junction. Hence, a high number of electrons are accumulated first (to overcome the barrier) before being injected into the ZnO triggering the abrupt current rise behaviour. During the reset process of the Ag/ZnO/Pt device, the joule heating effect plays a dominant role in inducing the abrupt current fall [25].

We further optimized our fabrication process based on Ag/ZnO/TiN configuration to reduce fabrication time and cost by reducing the thickness of ZnO to 35 nm and Ag TE to 5 or 15 nm; note that the deposition rate of ZnO is very slow (growth rate is approximately 0.01 Å/s) [26]. Decreasing the fabrication time and precious metal consumption beneficial for mass production, ensuring high process throughput and less energy consumption in the fabrication flow.

These devices were denoted as Au X/Ag X/ZnO X/TiN X; where the X represents the thickness of the respective films (in nm). The devices made with 15 nm of Au top electrode (without Ag) were also fabricated for comparison study. The I-V curves and endurance characteristics of these devices are shown in Fig. 3. Regardless of the thickness of the Ag layer, both of the Au/Ag/ZnO/TiN devices are able to show reproducible analogue switching behaviour (Fig. 3(a) and (b). However, the device made without Ag layer (Au/ZnO/TiN) is unable to reset (Fig. 3(c)); the employment of negative bias resulted in device breakdown. The switching process in Au/ZnO/TiN is controlled by the formation of a pure VoCF due to the absence of an Ag layer. The ability to switch On (set) but the inability to switch Off (reset) indicates that the size of VoCF connecting the BE and TE is excessively large, and a negative bias after a set process further leads to an even larger VoCF; consequently, this process increases the current flow in the device, and the device is stuck at the LRS [27]. Nevertheless, this behaviour is suitable for making write-once-read-many-times memory (WORM); WORM is a permanent data storage, and its non-erasable properties guarantee no data alteration that is useful for several applications such as RFID, electronic voting, artwork copyright protection, etc. [28], [29].

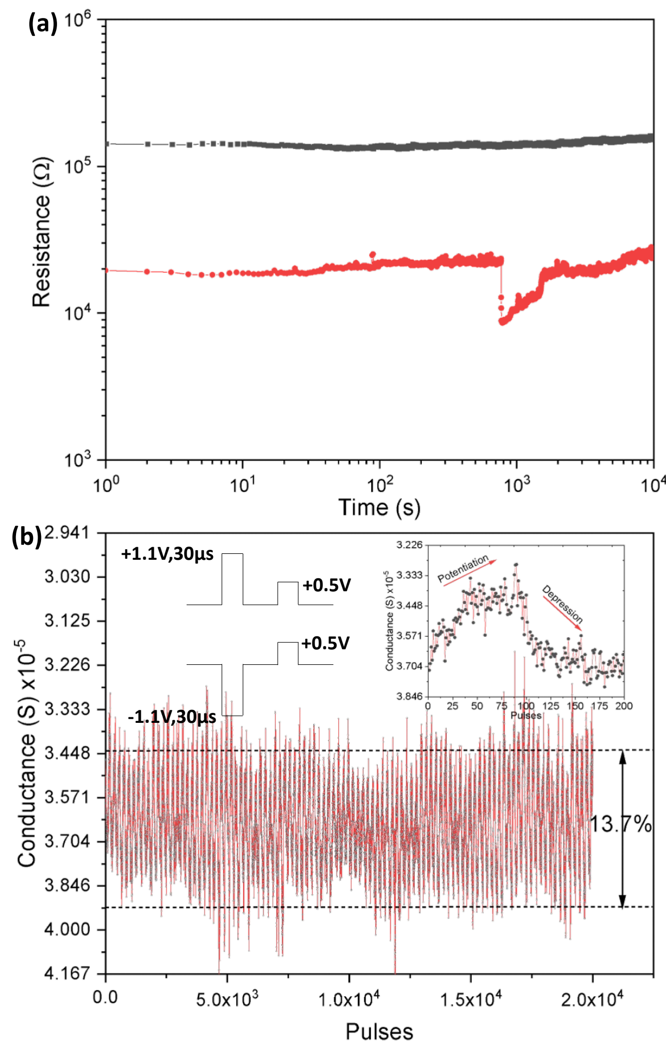

Fig. 4. (a) Room temperature retention and (b) synaptic performance of Au/Ag/ZnO/TiN device. A pulse scheme of 1.1V and -1.1V amplitude with the width of 30 us for each pulse was employed to induce potentiation and depression; a small amplitude of 0.5V was used as a read pulse. Inset in (b) shows the characteristic of a single epoch.

The device made with a very thin (5 nm) Ag layer TE exhibits unstable switching behaviour (Fig. 3 (d)). Some LRS and HRS states are overlapped, and there is no clear distinction between On and Off currents. Meanwhile, the device made with a thicker (15 nm) Ag layer TE performs decent switching endurance with an On/Off ratio of 5.6 times (Fig. 3(e)). We suggest that a sufficient thickness of the Ag layer is necessary to ensure there is enough Ag cation supply injected into the switching layer to form a conductive bridge; hence, the switching process is fully controlled by the rejuvenation and rupture of AgCB. However, when there is not enough Ag supply, the oxygen vacancies could also take part in the switching conduction leading to the competition between the redox process of Ag metal-cations and oxygen-oxygen oxygen vacancies during the switching process.

The switching instability of the Au5/Ag5/ZnO35/TiN60 device is useful for making low-powered random number generators (RNG). Each switching process produces unpredictable data (random LRS and HRS current levels (Fig. 3(d)), and this characteristic are suitable for generating one-time random passwords for security applications [15]. The Au5/Ag15/ZnO35/TiN60 device, on the other hand, has a sufficient On/Off ratio and good endurance, indicating its potential application for erasable (re-writeable) data storage. A retention test was conducted to confirm the non-volatility of the device, and the result is shown in Fig. 4(a). The device is able to maintain its LRS and HRS states for more than 104 seconds confirming good nonvolatile behaviour [30].

The Au5/Ag15/ZnO35/TiN60 device performs analogue switching (Fig. 3(b)). To exploit this analogue behaviour for synaptic applications, a potentiation and depression test was carried out. Fig. 4(b) shows the epoch endurance of the device; each epoch is generated by 200 repeated pulses of potentiation and depression. The device performs excellent endurance for more than $2x10^4$ pulses with a dynamic range of 13.7%. This result indicates the Ag/ZnO/TiN device structure is a good candidate for making robust neuromorphic computing elements [12].

IV. CONCLUSION

Device optimization was carried out employing an electrode engineering approach. We are able to control digital-to-analogue switching by utilizing an oxidizable and low work function electrode to encourage Ohmic contact, which avoids abrupt current changes during the switching process. An ultra-thin and moderate thickness of the top electrode results in non-uniform and stable endurance, respectively. On the other hand, the employment of an inert top electrode induces a single write characteristic with no ability to erase the data. Further optimization, tests, and device integration are being carried out and will be reported in the future.

ACKNOWLEDGMENT

This work is supported by MSCA EC Grant Agreement Number 101029535– MENESIS, FORTE, and RAEng CiET.

REFERENCES

[1] R. Aluguri, D. Kumar, F. M. Simanjuntak, and T.-Y. Tseng, "One bipolar transistor selector - One resistive random access memory device for cross bar memory array," *AIP Adv.*, vol. 7, no. 9, p. 095118, Sep. 2017.

[2] S. Salahuddin, K. Ni, and S. Datta, "The era of hyper-scaling in electronics," *Nat. Electron.*, vol. 1, no. 8, pp. 442–450, Aug. 2018.

[3] M. A. Zidan, J. P. Strachan, and W. D. Lu, "The future of electronics based on memristive systems," *Nat. Electron.*, vol. 1, no. 1, pp. 22–29, Jan. 2018.

[4] D. J. Wouters, R. Waser, and M. Wuttig, "Phase-Change and Redox-Based Resistive Switching Memories," *Proc. IEEE*, vol. 103, no. 8, pp. 1274–1288, 2015.

[5] S. Chandrasekaran, F. M. Simanjuntak, and T. Tseng, "Controlled resistive switching characteristics of ZrO 2 -based electrochemical metallization memory devices by modifying the thickness of the metal barrier layer," *Jpn. J. Appl. Phys.*, vol. 57, no. 4S, p. 04FE10, Apr. 2018.

[6] C.-F. Chang *et al.*, " Direct Observation of Dual-Filament Switching Behaviors in Ta 2 O 5 -Based Memristors ," *Small*, vol. 13, no. 15, p. 1603116, 2017.

[7] I. Valov and M. N. Kozicki, "Cation-based resistance change memory," *J. Phys. D. Appl. Phys.*, vol. 46, no. 7, p. 74005, 2013.

[8] J. Y. Chen, C. W. Huang, C. H. Chiu, Y. T. Huang, and W. W. Wu, "Switching Kinetic of VCM-Based Memristor: Evolution and Positioning of Nanofilament," *Adv. Mater.*, vol. 27, no. 34, pp. 5028–5033, 2015.

[9] D. M. Nminibapiel *et al.*, "Characteristics of Resistive Memory Read Fluctuations in Endurance Cycling," *IEEE Electron Device Lett.*, vol. 38, no. 3, pp. 326–329, 2017.

[10] Y. Sun, D. Wen, and X. Bai, "Nonvolatile ternary resistive switching memory devices based on the polymer composites containing zinc oxide nanoparticles," *Phys. Chem. Chem. Phys.*, vol. 20, no. 8, pp. 5771–5779, 2018.

[11] J. Prinzie, F. M. Simanjuntak, P. Leroux, and T. Prodromakis, "Low-power electronic technologies for harsh radiation environments," *Nat. Electron.*, vol. 4, no. 4, pp. 243–253, Apr. 2021.

[12] L.-Y. Chang, F. M. Simanjuntak, C.-L. Hsu, S. Chandrasekaran, and T.-Y. Tseng, "Suboxide interface induced digital-to-analog switching transformation in all Ti-based memristor devices," *Appl. Phys. Lett.*, vol. 117, no. 7, p. 073504, Aug. 2020.

[13] Q. Xia and J. J. Yang, "Memristive crossbar arrays for brain-inspired computing," *Nat. Mater.*, vol. 18, no. 4, pp. 309–323, 2019.

[14] F. M. Simanjuntak, S. Chandrasekaran, C.-C. Lin, and T.-Y. Tseng, "Switching Failure Mechanism in Zinc Peroxide-Based Programmable Metallization Cell," *Nanoscale Res. Lett.*, vol. 13, no. 1, p. 327, Dec. 2018.

[15] M. Lanza *et al.*, "Memristive technologies for data storage, computation, encryption, and radio-frequency communication," *Science (80-.).*, vol. 376, no. 6597, Jun. 2022.

[16] F. M. Simanjuntak, D. Panda, K. H. Wei, and T. Y. Tseng, "Status and Prospects of ZnO-Based Resistive Switching Memory Devices," *Nanoscale Res. Lett.*, vol. 11, no. 1, 2016.

[17] R. Waser, R. Dittmann, G. Staikov, and K. Szot, "Redox-Based Resistive Switching Memories - Nanoionic Mechanisms, Prospects, and Challenges," *Adv. Mater.*, vol. 21, no. 25–26, pp. 2632–2663, Jul. 2009.

[18] A. Saleem, F. M. Simanjuntak, S. Chandrasekaran, S. Rajasekaran, T.-Y. Tseng, and T. Prodromakis, "Transformation of digital to analog switching in TaOx-based memristor device for neuromorphic applications," *Appl. Phys. Lett.*, vol. 118, no. 11, p. 112103, Mar. 2021.

[19] Y. Xi *et al.*, "In-memory Learning with Analog Resistive Switching Memory: A Review and Perspective," *Proc. IEEE*, vol. 109, no. 1, pp. 14–42, Jan. 2021.

[20] J. A. Dean, *Lange's Handbook of Chemistry*, 15th ed., vol. 68, no. 6. New York: McGraw-Hill, 1999.

[21] L.-C. Chang, H.-L. Kao, and K.-H. Liu, "Effect of annealing treatment on the electrical characteristics of Pt/Cr-embedded ZnO/Pt resistance random access memory devices," *J. Vac. Sci. Technol. A Vacuum, Surfaces, Film.*, vol. 32, no. 2, p. 02B119, Mar. 2014.

[22] Z. Li, T. Schram, T. Witters, J. Tseng, S. De Gendt, and K. De Meyer, "Oxygen incorporation in TiN for metal gate work function tuning with a replacement gate integration approach," *Microelectron. Eng.*, vol. 87, no. 9, pp. 1805–1807, 2010.

[23] Y. C. Yang, F. Pan, F. Zeng, and M. Liu, "Switching mechanism transition induced by annealing treatment in nonvolatile Cu/ZnO/Cu/ZnO/Pt resistive memory: From carrier trapping/detrapping to electrochemical metallization," *J. Appl. Phys.*, vol. 106, no. 12, p. 123705, 2009.

[24] H. B. Michaelson, "The work function of the elements and its periodicity," *J. Appl. Phys.*, vol. 48, no. 11, pp. 4729–4733, Nov. 1977.

[25] S. Rajasekaran *et al.*, "Fast, Highly Flexible, and Transparent TaO x -Based Environmentally Robust Memristors for Wearable and Aerospace Applications," *ACS Appl. Electron. Mater.*, vol. 2, no. 10, pp. 3131–3140, Oct. 2020.

[26] F. M. Simanjuntak, T. Ohno, and S. Samukawa, "Influence of rf sputter power on ZnO film characteristics for transparent memristor devices," *AIP Adv.*, vol. 9, no. 10, p. 105216, Oct. 2019.

[27] F. M. Simanjuntak, T. Ohno, and S. Samukawa, "Film-Nanostructure-Controlled Inerasable-to-Erasable Switching Transition in ZnO-Based Transparent Memristor Devices: Sputtering-Pressure Dependency," *ACS Appl. Electron. Mater.*, vol. 1, no. 11, pp. 2184–2189, Nov. 2019.

[28] A. H. N. Melo and M. A. Macêdo, "Permanent Data Storage in ZnO Thin Films by Filamentary Resistive Switching," *PLoS One*, vol. 11, no. 12, p. e0168515, Dec. 2016.

[29] D. K. Maiti *et al.*, "Composition-dependent nanoelectronics of amido-phenazines: nonvolatile RRAM and WORM memory devices," *Sci. Rep.*, vol. 7, no. 1, pp. 1–10, 2017.

[30] H. J. Wan *et al.*, "Retention-failure mechanism of TaN∕Cu[sub x]O∕Cu resistive memory with good data retention capability," *J. Vac. Sci. Technol. B Microelectron. Nanom. Struct.*, vol. 27, no. 6, p. 2468, 2009.